Design and Evaluation of Filterless RGB Sensor on Standard CMOS Process

Takaya Sugiura, *Member, IEEE*, Hiroki Miura, and Nobuhiko Nakano, *Member, IEEE*

***Abstract*—In this study, a color detection phenomenon that does not utilize color filters is evaluated via the standard CMOS process. The device comprises multiple pn-junctions stacked in the depth direction, which enable division of the light responses by different light absorptions with respect to wavelength. To eliminate the color filters, we use rectifiers to cut the reverse currents corresponding to the long-wavelength infrared (Ir) regions. Numerical simulations predict the dynamic range of the sensor as 160 dB after removal of the filters that can decrease this value. Applications based on the Internet of Things can be realized via mass production at low cost by eliminating the additional processes required to form the conventional color filters in front of the sensor. We evaluate the proposed device by both numerical simulation and experiment as well as clarify that the sensing phenomenon requires sufficient PWell thickness to separate the depletion regions for successful operation. The appropriate process parameters for the CMOS process are revealed, providing useful information for testing under a wide range of process conditions.**

***Index Terms*—CMOS process, color sensing, IoT, LSI, numerical simulation, TCAD.**

I. Introduction

A PHOTODIODE is a common photonic device used to detect the presence of light. Photodiodes are employed in devices such as CMOS image sensors, which are one of their major applications [1]. CMOS image sensors use color filters to distinguish the wavelength of light; multiple photodiode devices are often required to realize this function, and at least three photodiodes are required to obtain RGB information. This may lead to overuse of the sensor area or increased power consumption of the entire system.

The standard CMOS process generally employed in digital/analog IC manufacturing has several diffusion layers or metals to realize the integration of several semiconductor devices on a chip, such as transistors, diodes, resistors, capacitors, and inductors. By designing a pn-junction using the available diffusion layers, the photovoltaic cells can be integrated into such chips [2]–[8]. This enables integration of transistors (system block) and photovoltaic cells (energy source) on a chip [9], which is widely suitable for Internet of Things (IoT) applications [10], [11]. These layers are also hierarchical, enabling the formation of multiple pn-junctions in the depth direction. As light of longer wavelength is absorbed in the deeper regions of the semiconductor, the structure can distinguish wavelengths via the current values from each contact.

Several silicon-based RGB sensors [12]–[14] have been developed; these sensors rely on infrared (Ir) filters to achieve improved sensing accuracy. Because of the bandgap energy of 1.12 eV in silicon, silicon-based devices also react to Ir illumination until the wavelength reaches about 1 μm, and state-of-the-art sensors still utilize Ir filters to eliminate it [15], [16]. Because formation of an Ir filter requires additional processes, it may not be suitable for low-cost mass production. There is an alternative method that utilizes a germanium compound, whose bandgap energy is much lower than that of silicon and below 1 eV, to control color responses [17]; however, the use of germanium is incompatible with existing system LSIs.

In this study, a single-device filterless color divider designed using the standard CMOS process is proposed. The device does not need both the RGB filters and Ir filter for RGB sensing. The RGB filters are therefore removed by stacking multiple pn-junctions, and the Ir filter is removed using rectifiers such as diodes. This implementation is easily accomplished through integration with the standard CMOS process. Experiments show that the operation of the proposed device is affected by the process parameters. Hence, an additional numerical simulation was performed to determine the details of sensor operation and provide appropriate process parameters. Penetration of the depletion region is critical for sensor operation; therefore, shrinking the depletion region or enhancing the layer thickness should be considered.

II. Device Characterization

The concept of the CMOS process integrated color divider is shown in Fig. 1. The device comprises multiple pn-junctions and three pn-diodes in its structure. The pn-junction can separate the generated carriers; therefore, the wavelength response can be distinguished by stacking the pn-junctions alternately. The pn-junctions are located at different depths; the diodes near the surface respond to shorter wavelengths of light, and the diodes in the deeper regions only respond to light of longer wavelengths. Because Si has a bandgap of approximately 1.1 eV, it covers the visible light wavelength band and is useful for RGB sensors. Using this property, the wavelengths are distinguished by monitoring the photocurrents of each of the diodes.

Manuscript received April 14, 2022; revised May 24, 2022; accepted May 25, 2022. Date of publication May 30, 2022; date of current version June 13, 2022. This work was supported by the VLSI Design and Education Center of the University of Tokyo in collaboration with Synopsys, Inc. *(Corresponding author: Takaya Sugiura.)*

The authors are with the Department of Electronics and Electrical Engineering, Keio University, Yokohama, Kanagawa 223-8522, Japan (e-mail: takaya_sugiura@nak.elec.keio.ac.jp; hmiura@nak.elec.keio.ac.jp; nak@elec.keio.ac.jp).

Digital Object Identifier 10.1109/JPHOT.2022.3178833

This work is licensed under a Creative Commons Attribution 4.0 License. For more information, see https://creativecommons.org/licenses/by/4.0/

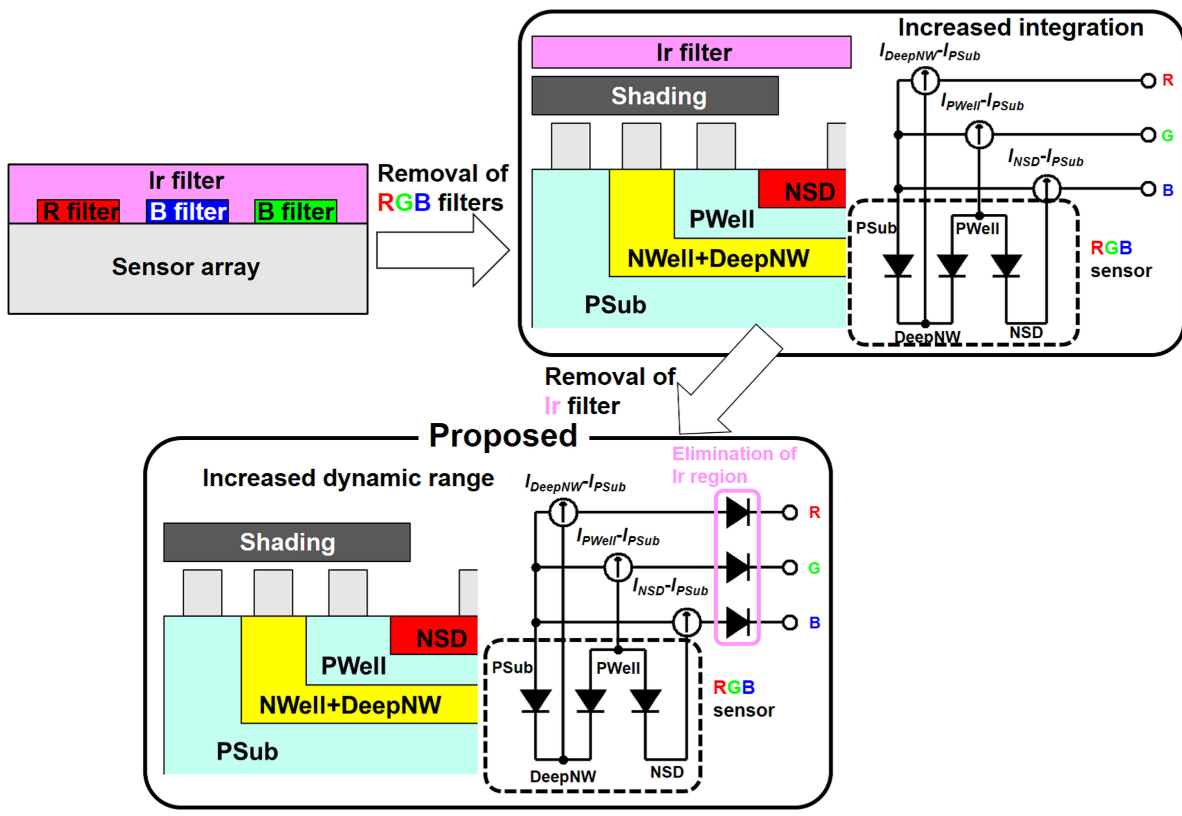

Fig. 1. Concept of on-chip filterless color divider: device structure and equivalent circuit from the conventional to the proposed sensor.

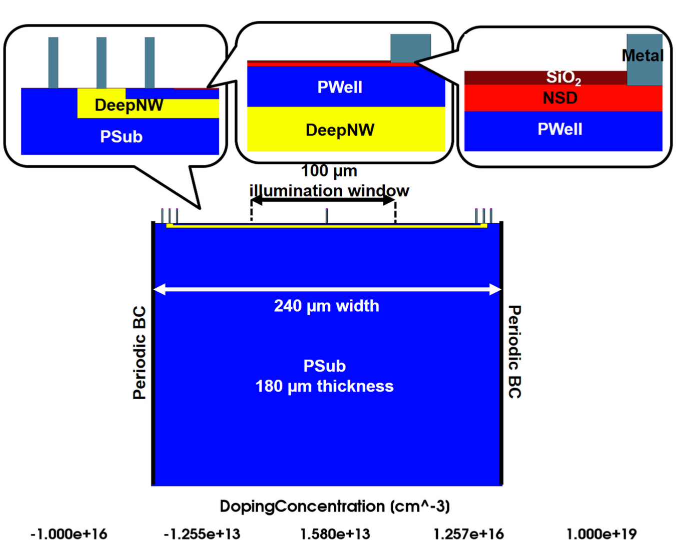

Fig. 2. Simulation model of the RGB sensor with 2D grid.

While some previous works have utilized multiple pn-junctions to divide the light responses, our proposed sensor is based on the Bi-CMOS technology [12], and an Ir filter is necessary to improve the sensing accuracy [12]–[14]. The Ir responses become dominant with thicker substrate regions, and the small amount of light energy increases the number of generated carriers more than light of short wavelengths. Therefore, elimination of the Ir regions can be problem when avoiding false positives. The proposed sensor avoids the use of Ir filters that need additional processes; instead, we use rectifiers such as diodes to cut the reverse currents corresponding to the Ir region. These diode connections can be easily achieved through implementation using the standard CMOS process.

TABLE I
PHYSICAL VALUES USED FOR SIMULATION MODELING IN THIS STUDY

Physics	Value
Material	Silicon
Device thickness [μm]	180
NSD depth [nm]	100
PWell depth [μm]	1
DeepNW depth [μm]	3
Bulk resistivity [Ω-cm]	1.47
Bulk lifetime [μs] [18]	500
Complex refractive index [19]	M. A. Green's data in 2008

III. NUMERICAL SIMULATION

A. Simulation Modeling

Sentaurus Technology-Computer-Aided-Design (TCAD) software provided by Synopsys, Inc. [20] was used for the simulation. The simulation modeling was based on a two-dimensional component, where the X- and Y-directions correspond to the lateral and depth directions, respectively. The simulation model is shown in Fig. 2, where the stacked pn-junctions are formed on the front side. The simulation parameters used in this study are listed in Table I. Here,

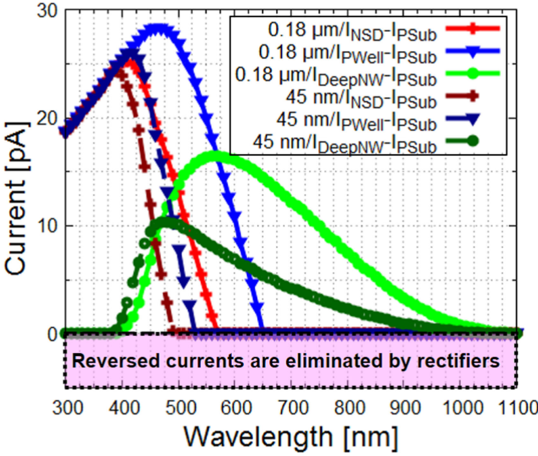

Fig. 3. Wavelength–current responses with two CMOS processes and their contact current differences.

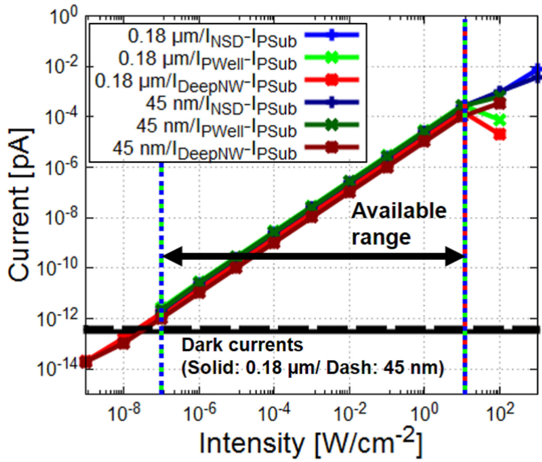

Fig. 4. Intensity-dependent current of each CMOS process for R, G, and B colors.

information regarding the substrate in the depth direction, which is not directly related to the circuit design, is not disclosed to the designer. Therefore, we have used general values for the device modeling in this study.

As default settings, the illumination light intensity was maintained at 1 μW/cm^2, and p-contacts were 500 mV reverse biased. Moreover, only the center area above the NSD region was open for light illumination (this helps realize wavelength discrimination and CMOS process confinement of the DUMMY metal area).

B. Simulation-Based Evaluation

We evaluated the standard CMOS process with gate lengths of 0.18 μm [21] and 45 nm [22] using the process parameters available in literature. Here, to focus on the well (PWell and DeepNW) phenomena and safe parameters, the bulk resistivity noted in Table I is used. Fig. 3 shows the wavelength–current responses for the two CMOS processes, from which the current value difference of each contact with the PSub contact is obtained (as the absolute value). Here, the negative value is eliminated, which is easily achieved in the device by connecting diodes to the outputs. It is shown that the elimination of the reverse currents adequately emphasizes the current peaks with different wavelengths for each contact. As shown in the graph, the proposed sensor structure can be applied to RGB sensing by considering the current value differences, so that the NSD, PWell, and DeepNW correspond to short (blue), middle (green), and long (red) light wavelengths, respectively. The shrunken CMOS process shifts the peaks toward the direction of shorter wavelengths; therefore, the legacy CMOS process is favorable for RGB sensing.

Fig. 4 shows the intensity dependency of each CMOS process for the R, G, and B colors. This is independent from the CMOS process, and the lower limit of G and B are observed at 10^{-7} W/cm^2, while the higher limit is at 10 W/cm^2. The dynamic range is thus calculated as $20\log_{10}(10/10^{-7}) = 160$ dB. The

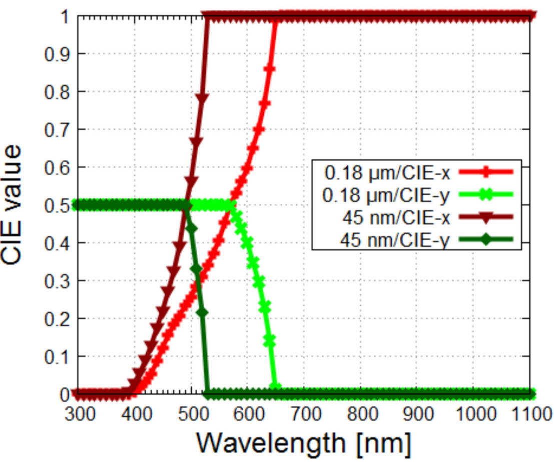

Fig. 5. CIE value of each CMOS process at a light intensity of 1 μW/cm^2.

dynamic range of a mainstream CMOS image sensor is approximately 110 dB [23]; thus, the proposed structure provides comparatively superior performance. It can also be considered that the filterless structure senses more light by avoiding attenuation at the filters, thereby providing a higher dynamic range.

Fig. 5 shows the CIE value of each CMOS process. Here, the CIE values are calculated as the ratios of the currents of the red or green wavelengths to the total sum of the current. It is observed that the 0.18 μm process is closer to the peak of each color. The introduction of rectifiers eliminates the values outside the range of interest to zero.

IV. EXPERIMENT

The proposed color detector was designed using a 0.18 μm standard CMOS process provided by Rohm Co., Ltd. Fig. 6 shows the layout of the proposed color sensing device; the light aperture is of size 50 μm $\times$ 50 μm and comprises one line-shaped and three ring-shaped contacts. Each terminal is

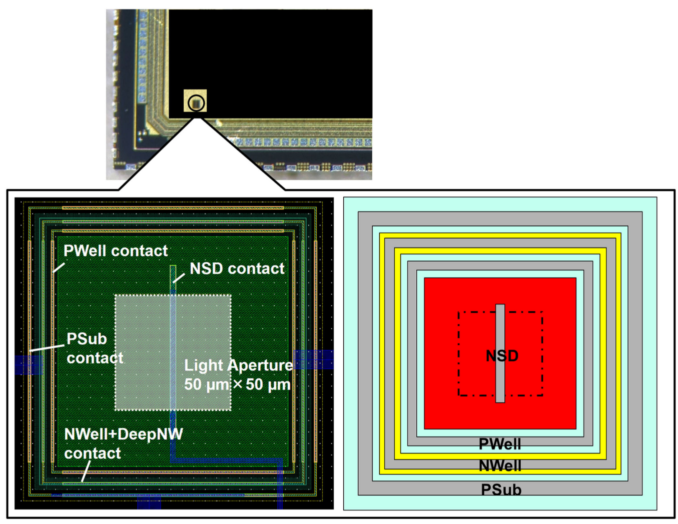

Fig. 6. Photograph of the entire chip and layout data of the proposed color sensing device.

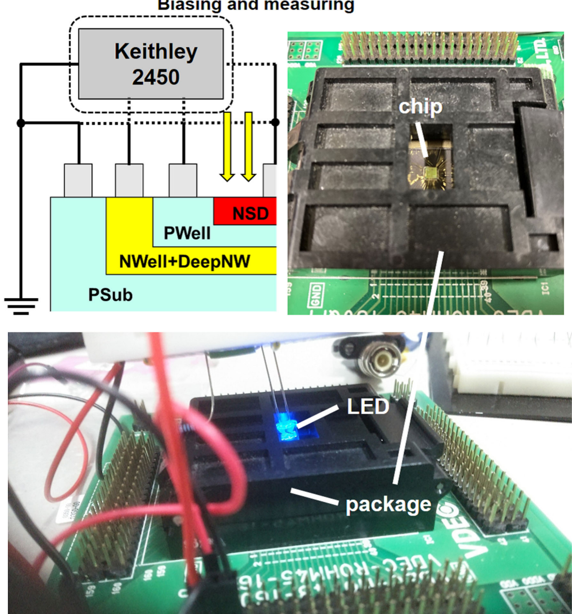

Fig. 7. Experimental setup: chip pad for biasing and prototyping board for LED illumination.

interconnected to the bonding wire, which is in contact with the chip pad. Fig. 7 shows a photograph of the experimental setup used in this study. The experimental setup comprises a chip pad for biasing, a Tektronix Keithley 2450 source meter for measurements, and a prototyping board with LEDs for light illumination. One terminal was connected to the source meter for biasing, and the others were connected to ground. The LEDs used in this experiment were L5-EKR2530-12500 (red) [24], L5-G2530-20000 (green) [25], and BL503B2CA1A01 (blue) [26], manufactured by Linkman Co., Ltd. The LEDs were driven by a 3 V battery with a 1 kΩ series resistance.

Fig. 8 shows the biased operation of each terminal under black, red, green, and blue light illumination. Here, all the

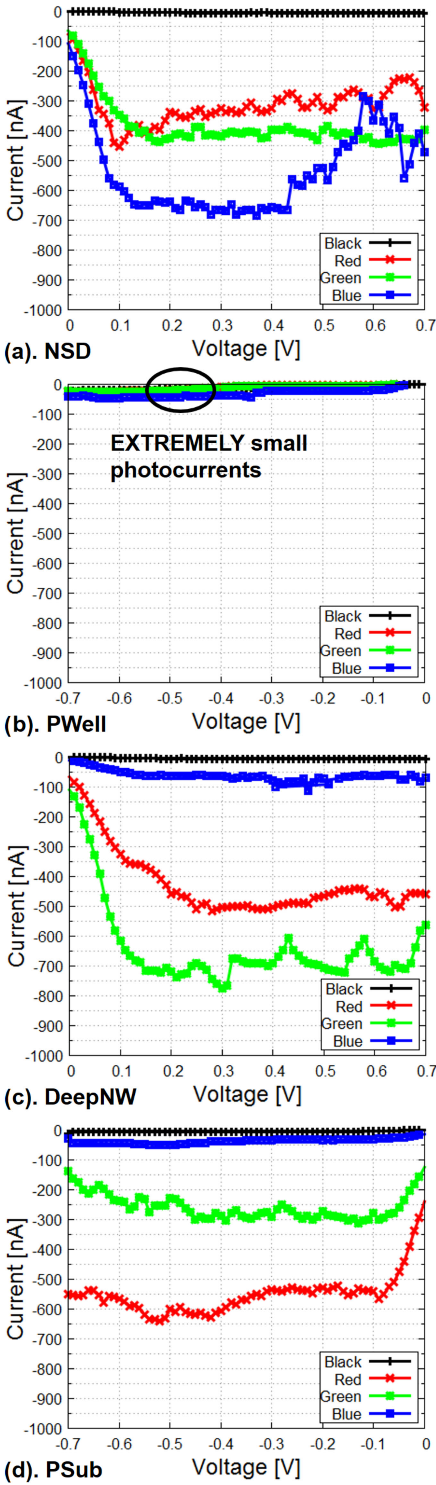

Fig. 8. Reverse-bias operations of the four terminals for the four illumination lights: (a) NSD, (b) PWell, (c) DeepNW, and (d) PSub.

terminals were biased to enlarge the depletion region. An important issue here is the extremely small photocurrent in the PWell contact, which is almost equal to the black condition, with values more than 10 times smaller than the photocurrents of the other contacts. This phenomenon makes it difficult to

use the sensor for RGB sensing because the PWell contact should correspond to the middle-range wavelength of light, i.e., green. From a general viewpoint, these extremely small PWell currents may be problematic; therefore, we focus on phenomena that demonstrate the proposed sensor to be unsuitable for RGB sensing from the perspective of a numerical simulation.

V. Process Parameters

Fig. 9 shows the wavelength–current response of each contact when the PWell thickness is varied. Here, the fundamental process parameters are based on the 0.18 μm CMOS process. The variation of the PWell thickness revealed that a thin PWell affects sensor operation at a critical level. An extremely small PWell current is also observed when the PWell is too thin (under 0.4 μm), with the result strongly corresponding to that of the experiment (Fig. 8), suggesting that the process parameters used in our experiment are NOT suitable for RGB sensing. The results also suggest that the generated carriers pass through the PWell region, thus making it difficult to detect the color responses at each contact. Other than the PWell, the NSD response is affected drastically; the peak wavelength in the Ir region shifts, the peak in DeepNW drops, and PSub responds to a wider range of wavelengths, including shorter wavelengths. Considering this malfunction in the case of the thin PWell, it is noted that the depletion regions in the PWell–DeepNW regions are insufficient for essential carrier separation.

We next focus on the PWell and DeepNW process parameters, including thickness and concentration. Fig. 10 shows a mapping of the process parameter evaluations by varying the PWell and DeepNW conditions. To judge the suitability of the process parameters, we consider whether I_{NSD}/I_{PSub} is larger than 10 based on the results in Fig. 10; when $I_{NSD}/I_{PSub} > 10$, the process parameters are judged to be good. This evaluation includes the bulk resistivity of the light-doped (bulk concentration 1×10^{16} cm^{-3}) and heavy-doped (bulk concentration 1×10^{18} cm^{-3}) regions. The results show that the bulk resistivity is almost negligible and that a thick PWell is suitable for good fabrication.

Finally, we evaluated the phenomena in the well regions, including space charge and electrostatic potential, which are essential for sensor operation. Figs. 11 and 12 show the space charge and electrostatic potential plots for each well doping concentration (10^{15}, 10^{16} and 10^{17} cm $^{-3}$ at PWell and DeepNW) for a PWell thickness of 0.5 μm and DeepNW thickness of 1 μm. A wavelength of 400 nm is considered in this evaluation. From Fig. 10, the condition of 10^{15} cm^{-3} is not suitable for RGB sensing, and heavier concentrations are required. The space charge plots show that the “Bad” process parameters allow penetration of the depletion regions. Hence, they are unable to separate the carriers and pass them to the substrate region corresponding to a large PSub current. In contrast, the “Good” process parameters result in space charge decrease in the DeepNW region, preventing carriers from escaping from the well regions. In addition, the electrostatic potential plot shows that the “Bad” process parameters result in a monotonous decline from the NSD to PSub that passes carriers to the substrate,

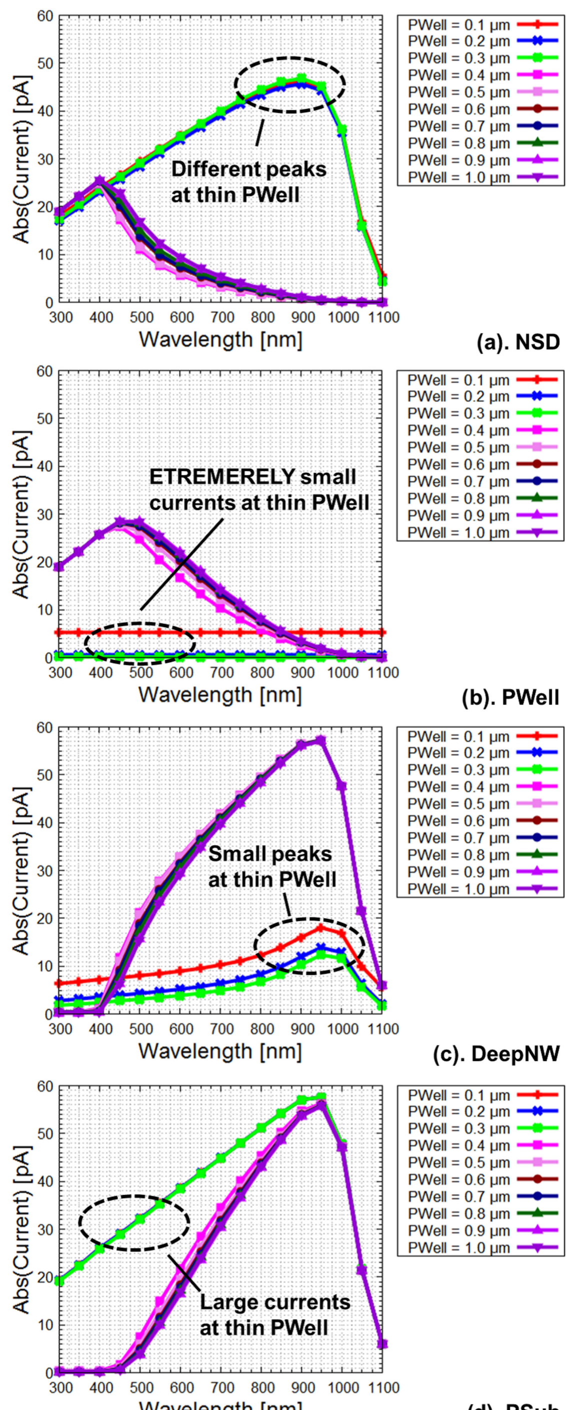

Fig. 9. Wavelength–current responses with the two CMOS processes and their contact current differences.

contrary to the “Good” parameters allowing inverted potentials in the well regions that are necessary for carrier separation.

As a consequence, the separation of the depletion regions in the well regions is a key consideration for RGB sensing, and the process parameters including doping concentration and thickness are important. Heavier doping thins the depletion region, and thicker well regions are favorable. In addition, the effects of

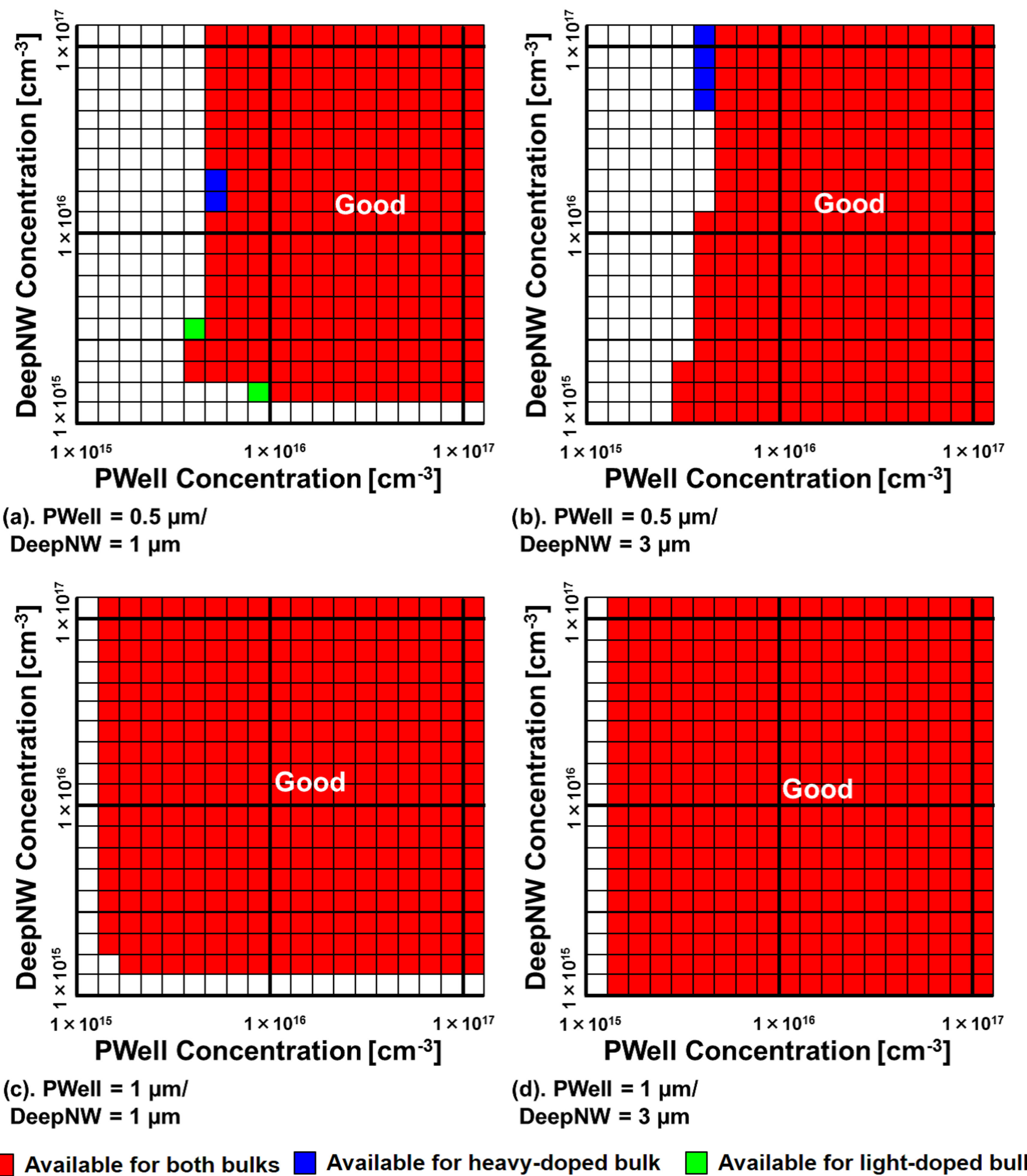

Fig. 10. Mappings of the availability of the process parameters for RGB sensing.

the PWell region are dominant, and the current becomes almost zero for the “Bad” condition; both the doping concentration and thickness have large effects on the operation. As the bulk resistivity is negligible, the choice of the bulk material can be made freely; however, the settings of the process parameters must be considered.

VI. Conclusion

We propose a single-device color detector without filters that can be manufactured using standard CMOS processes. The removal of the RGB and Ir filters contribute to improved integration and dynamic range, and a 160 dB dynamic range was predicted by numerical simulation. Although the experiments did not show favorable operation, analysis of the numerical simulations revealed detailed sensor operation phenomena and provided design guidelines to realize RGB sensing via standard CMOS processes. The connections of the depletion regions in the well regions are critical for RGB sensing so that carriers are passed to the substrate. The design of the well regions, especially the PWell, is thus important, and the implementation of the PWell with heavier doping and greater thickness is a key area for further development.

Acknowledgment

The VLSI chip used in this study was fabricated in the chip fabrication program through the activities of the VDEC

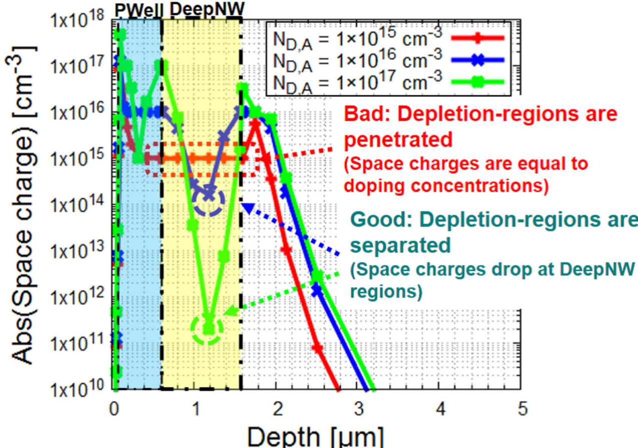

Fig. 11. Space charge plots in the depth direction for each well doping concentration.

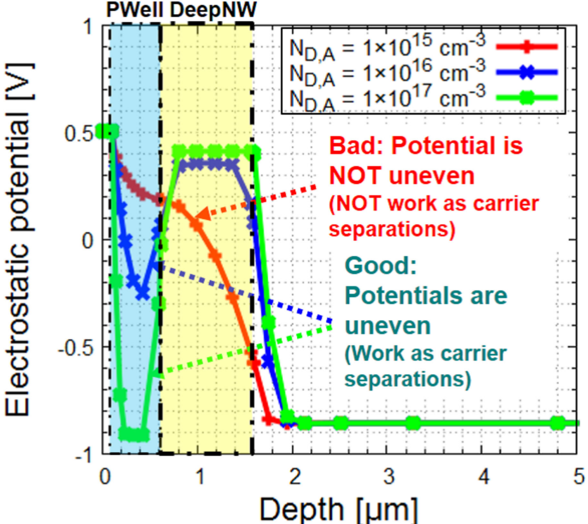

Fig. 12. Electrostatic potential plots in the depth direction for different well doping concentrations.

in collaboration with Rohm Corporation and Toppan Printing Corporation.

References

[1] P. C. Eng, S. Song, and B. Ping, "State-of-the-art photodetectors for optoelectronic integration at telecommunication wavelength," *Nanophotonics*, vol. 4, no. 3, pp. 277–302, Oct. 2015. [Online]. Available: https://doi.org/10.1515/nanoph-2015-0012

[2] Y. Arima and M. Ehara, "On-chip solar battery structure for CMOS LSI," *IEICE Electron. Exp.*, vol. 3, no. 13, pp. 287–291, Jul. 2006. [Online]. Available: https://doi.org/10.1587/elex.3.287

[3] I. Mori, M. Kubota, E. Lebrasseur, and Y. Mita, "On-chip high-voltage silicon photovoltaic cell array made by a CMOS post-processed device isolation method for driving a MEMS actuator in a remote manner," *IEEJ Trans. Sensor Micromachines*, vol. 136, no. 2, pp. 24–30, Feb. 2016. [Online]. Available: https://doi.org/10.1541/ieejsmas.136.24

[4] F. Horiguchi, "Integration of series-connected on-chip solar battery in a triple-well CMOS LSI," *IEEE Trans. Electron. Devices*, vol. 59, no. 6, pp. 1580–1584, Jun. 2012. [Online]. Available: https://doi.org/10.1109/TED.2012.2189116

[5] M. K. Law and A. Bernak, "High-voltage generation with stacked photodiodes in standard CMOS process," *IEEE Electron. Device Lett.*, vol. 31, no. 12, pp. 1425–1427, Dec. 2010. [Online]. Available: https://doi.org/10.1109/LED.2010.2075910

[6] Y. Hung, M. Cai, and H. Su, "High-voltage generation in CMOS photovoltaic devices by localized substrate removal," *IEEE Electron. Device Lett.*, vol. 37, no. 6, pp. 754–757, Jun. 2016. [Online]. Available: https://doi.org/10.1109/LED.2016.2550496

[7] C. Steffan, P. Greiner, B. Deutschmann, C. Kollegger, and G. Holweg, "Energy harvesting with on-chip solar cells and integrated DC/DC converter," in *Proc. 45th Eur. Solid-State Device Res. Conf.*, 2015, pp. 142–145. [Online]. Available: https://doi.org/10.1109/ESSDERC.2015.7324733

[8] Y. Hung, T. Chuang, C. Chunn, L. Yang, and S. Lee, "Interdigitated back-contact solar cells implemented with foundry CMOS processes," in *Proc. Conf. Lasers Electron.-Opt. - Laser Sci. Photon. Appl.*, 2014, pp. 1–2. [Online]. Available: https://doi.org/10.1364/CLEO_AT.2014.JW2A.1

[9] K. Igarashi, Y. Minami, and N. Nakano, "Heterogeneous integration of boost power supply and on-chip solar cell using triple well CMOS process," *IEEJ Trans. Electron. Inf. Syst.*, vol. 138, no. 1, pp. 41–49, Jan. 2018. [Online]. Available: https://doi.org/10.1541/ieejeiss.138.41

[10] D. Spirjakin, A. M. Baranov, and V. Sleptsov, "Design of smart dust sensor node for combustible gas leakage monitoring," in *Proc. Fed. Conf. Comput. Sci. Inf. Syst*., 2015, pp. 1279–1283. [Online]. Available: https://doi.org/10.15439/2015F172

[11] J. Gubbi, R. Buyya, S. Marusic, and M. Palaniswami, "Internet of Things (IoT): A vision, architectural elements, and future directions," *Future Gen. Comput. Syst.*, vol. 29, no. 7, pp. 1645–1660, Sep. 2013. [Online]. Available: https://doi.org/10.1016/j.future.2013.01.010

[12] M. B. Chouikha, G. N. Lu, M. Sedjil, G. Sou, and G. Alquie, "Buried triple P-N junction structure in a BiCMOS technology for color detection," in *Proc. Bipolar/BiCMOS Circuits Technol. Meeting*, 1997, pp. 108–111. [Online]. Available: https://doi.org/10.1109/BIPOL.1997.647408

[13] R. B. Merrill, "Color separation in an active pixel cell imaging array using a triple-well-structure," U.S. Patent 5,965,875, Oct. 1999.

[14] A. Rush and P. Hubel, "X3 sensor characteristics," *J. Soc. Photographic Sci. Technol. Jpn.*, vol. 66, no. 1, pp. 57–60, Feb. 2003. [Online]. Available: https://doi.org/10.11454/photogrst1964.66.57

[15] T. Woodstock and R. F. Karlicek, Jr., "RGB color sensors for occupant detection: An alternative to PIR sensors," *IEEE Sensors J.*, vol. 20, no. 20, pp. 12364–12373, Oct. 2020. [Online]. Available: https://doi.org/10.1109/JSEN.2020.3000170

[16] AMS AG, TCS34725 Color Sensor, [Online]. Available: https://ams.com/tcs34725

[17] M. Jafari, L. J. Guo, and M. Rais-Zadeh, "Waveguide grating color reflector using germanium telluride," in *Proc. 20th Int. Conf. Solid-State Sens. Actuators Microsystem Eurosensors XXXIII*, 2019, pp. 478–481. [Online]. Available: https://doi.org/10.1109/TRANSDUCERS.2019.8808283

[18] S. W. Glunz, S. Rein, J. Y. Lee, and W. Warta, "Minority carrier lifetime degradation in boron-doped Czochralski silicon," *J. Appl. Phys.*, vol. 90, no. 5, pp. 2397–2404, Aug. 2001. [Online]. Available: https://doi.org/10.1063/1.1389076

[19] M. A. Green, "Self-consistent optical parameters of intrinsic silicon at 300 K including temperature coefficients," *Sol. Energy Mater. Sol. Cells*, vol. 92, no. 11, pp. 1305–1310, Nov. 2008. [Online]. Available: https://doi.org/10.1016/j.solmat.2008.06.009

[20] "Synopsys TCAD Software Release L-2016.03-SP2," Sentaurus Device, Mountain View, CA, USA, 2016.

[21] B. Ciftcioglu *et al.*, "Integrated silicon PIN photodiodes using deep N-well in a standard 0.18-μm CMOS technology," *J. Lightw. Technol.*, vol. 27, no. 15, pp. 3303–3313, Aug. 2009. [Online]. Available: https://doi.org/10.1109/JLT.2008.2008664

[22] W. Zhi, Q. Quan, P. Yu, and Y. Jiang, "A 45 nm CMOS avalanche photodiode with 8.4-GHz bandwidth," *Micromachines*, vol. 11, no. 1, Art. no. 65, Jan. 2020. [Online]. Available: https://doi.org/10.3390/mi11010065

[23] T. Kim, "Wide dynamic range technologies: For mobile imaging sensor systems," *IEEE Consum. Electron. Mag.*, vol. 3, no. 2, pp. 30–35, Mar. 2014. [Online]. Available: https://doi.org/10.1109/MCE.2014.2298072

[24] Linkman Company, Ltd., L5-EKR2530-12500 [Online]. Available: https://www.linkman.jp/user/shohin.php?p=61068

[25] Linkman Company, Ltd., L5–G2530-20000, [Online]. Available: https://www.linkman.jp/user/shohin.php?p=61069

[26] Linkman Company, Ltd., BL503B2CA1A01, [Online]. Available: https://www.linkman.jp/user/shohin.php?p=58004